Journal of Industrial and Engineering Chemistry xxx (xxxx) xxx-xxx

Contents lists available at ScienceDirect

Journal of Industrial and Engineering Chemistry

journal homepage: www.elsevier.com

High-temperature oxidation of europium (II) sulfide

Yuriy G. Denisenko [a, b], Maxim S. Molokeev [c, d, e], Alexander S. Krylov [f], Aleksandr S. Aleksandrovsky [g, h], Aleksandr S. Oreshonkov [d, f], Victor V. Atuchin [i, j, k, l, *], Nikita O. Azarapin [a], Pavel E. Plyusnin [m], Elena I. Sal'nikova [a, n], Oleg V. Andreev [a]

[a] Department of Inorganic and Physical Chemistry, Tyumen State University, Tyumen 625003, Russia
[b] Department of General and Special Chemistry, Industrial University of Tyumen, Tyumen 625000, Russia
[c] Laboratory of Crystal Physics, Kirensky Institute of Physics, Federal Research Center KSC SB RAS, Krasnoyarsk 660036, Russia
[d] Siberian Federal University, Krasnoyarsk 660041, Russia
[e] Department of Physics, Far Eastern State Transport University, Khabarovsk 680021, Russia
[f] Laboratory of Molecular Spectroscopy, Kirensky Institute of Physics Federal Research Center KSC SB RAS, Krasnoyarsk 660036, Russia
[g] Laboratory of Coherent Optics, Kirensky Institute of Physics Federal Research Center KSC SB RAS, Krasnoyarsk 660036, Russia
[h] Institute of Nanotechnology, Spectroscopy and Quantum Chemistry, Siberian Federal University, Krasnoyarsk 660041, Russia
[i] Laboratory of Optical Materials and Structures, Institute of Semiconductor Physics, SB RAS, Novosibirsk 630090, Russia
[j] Functional Electronics Laboratory, Tomsk State University, Tomsk 634050, Russia
[k] Laboratory of Single Crystal Growth, South Ural State University, Chelyabinsk 454080, Russia
[l] Research and Development Department, Kemerovo State University, Kemerovo 650000, Russia
[m] Laboratory of Chemistry of Rare Platinum Metals, Nikolaev Institute of Inorganic Chemistry SB RAS, Novosibirsk, 630090, Russia
[n] Department of General Chemistry, Northern Trans-Ural Agricultural University, Tyumen, 625003, Russia

ARTICLE INFO

Article history:
Received 20 February 2019
Received in revised form 10 April 2019
Accepted 5 May 2019
Available online xxx

Keywords:
Sulfur-containing europium compounds
High-temperature oxidation
Thermal analysis
X-ray diffraction
Crystal structure
Photoluminescence

ABSTRACT

The process of high-temperature oxidation of EuS in the air was explored in the temperature range of 500–1000 °C. The oxidation reaction enthalpy was determined (ΔH^0_{exp}=——1718.5 kJ/mol). The study of oxidation products allowed to establish the mechanism of EuS oxidation with oxygen. At 500–600 °C, EuS is oxidized to a mixture of Eu^{3+}-containing compounds (Eu_3S_4, Eu_2O_2S). In the range of 700–1000 °C, only europium sulfate $Eu_2O_2SO_4$ is formed. The structure refinement for $Eu_2O_2SO_4$ was performed by the Rietveld method. The luminescence intensity of europium oxysulfate $Eu_2O_2SO_4$ with characteristic 4f-4f transitions from the $^5D_0$ state was investigated as a function of oxidation temperature.

Introduction

Oxygen-containing compounds of europium Eu^{3+} attracted researchers attention for a long time due to the effective red luminescence, which has found application in many optical systems [1–9]. In recent years, a number of studies were implemented on the synthesis of compounds with a stoichiometric europium content. The samples stoichiometry ensures the precise determination of the radiating ions crystallographic positions, and, as a result, it becomes possible to establish the influence of the coordination environment on the luminescent properties of Eu^{3+} ions [10–20]. Such self-activated phosphors are characterized by an almost complete absence of defects in the crystal structure. A qualitative description of the crystal structure allows tracking the influence of non-structural factors (synthesis temperature and time, particle size, etc.) on the luminescent-spectral properties.

Rare-earth oxidesulfates $Ln_2O_2SO_4$ exhibit a set of rather interesting magnetic properties [21–25]. The presence of sulfur as a redox center in oxysulfates determines their potential use as catalysts for the conversion process of water gas [26,27], solid oxide fuel cells and batteries [28,29], materials for storing gaseous oxygen [30–32]. Doped oxysulfates $(Ln_{1-x}Eu_x)_2O_2SO_4$ are promising for the use as highly efficient phosphors when excited by ultraviolet light or X-rays. The compounds enhanced their thermal stability and effective, reproducible luminescence characteristics [33–41]. However, to our best knowledge, the data on the structural and spectroscopic properties of stoichiometric europium oxysulfate $Eu_2O_2SO_4$ are absent in the literature.

As it is well known, thermal destruction methods are convenient for obtaining materials with different properties [42–49]. In the synthesis of compounds containing isolated sulfate groups $(SO_4)^{2-}$, the methods applied for the oxidation of compounds containing sulfur in the lowest oxidation state S^{2-} are of particular attention. According

* Corresponding author at: Institute of Semiconductor Physics, Novosibirsk 630090, Russia.
Email address: atuchin@isp.nsc.ru (V.V. Atuchin)

https://doi.org/10.1016/j.jiec.2019.05.006
1226-086/

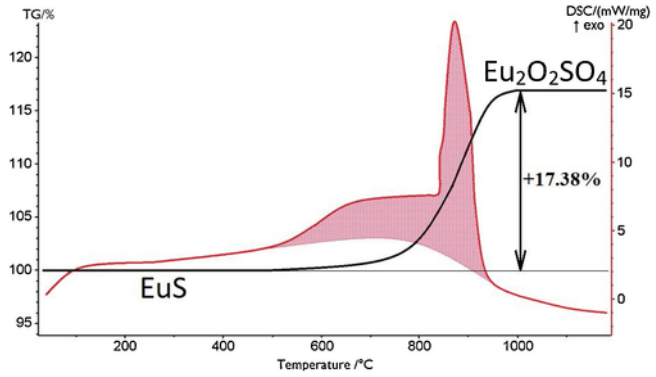

Fig. 1. DTA/TG of EuS in synthetic air.

to the data of [50], monosulfides of rare-earth elements are oxidized by air oxygen to oxysulfides Ln_2O_2S. Above this, various oxides Ln_xO_y appear as oxidation by-products. According to the data reported in Refs. [51–56], the oxysulfides Ln_2O_2S are unstable in the air at high temperatures and stoichiometric oxysulfates $Ln_2O_2SO_4$ are formed in this temperature range as the final reaction products. Comparatively, alkaline earth compounds MeS (Me = Ca, Sr, Ba) are oxidized with atmospheric oxygen to stoichiometric sulphates $MeSO_4$ [57–59]. The inconsistency of the data suggests that europium monosulfide EuS can be oxidized with atmospheric oxygen to stoichiometric sulfates, and the method can be used for controlled phosphor syntheses. Europium monosulfide can be obtained as nanoparticles of different shapes (nanocubes, nanowires, nanofibres, etc.), and it can be used as a precursor in the synthesis of nanoparticles of oxygen-containing Eu^{3+} compounds. Respectively, it is important to study the thermochemical transformation mechanism for europium monosulfide in the oxidizing air atmosphere and the possibility of targeted production of oxygen-containing Eu^{3+} compounds in this process. Thus, the present study is aimed at the exploration of EuS oxidation process in the air, including the structural and spectroscopic analysis of the reaction products.

Materials and methods

Synthesis

Europium monosulfide was synthesized from europium oxide Eu_2O_3 (ultrapure, 99.999%, TDM-72, Russia) in the reaction of high-temperature interaction with carbon disulfide CS_2 vapor (99.9%, Aldrich, France). According to the X-ray diffraction (XRD) results, the Eu_2O_3 reagent does not contain foreign crystalline impurities (Fig. S1.a) and it crystallizes in the cubic symmetry with the cell parameters listed in Table S1. The atomic coordinates and anisotropic thermal parameters (Table S2) are consistent with the literature data [60]. According to the scanning electron microscopy (SEM) data, europium oxide powder is formed by faceted particles with average sizes of 1–10 μm (Fig. S1.b). Argon (99.99999%, Sibtechnology, Russia) was used as a carrier gas. The experimental set up used for the EuS synthesis is shown in Figure S2. The carrier gas at a rate of 6 l/h was passed through a glass round-bottom flask with carbon disulfide, heated to 40 °C in a heating mantle. First, the argon flow carrying CS_2 vapor was passed through a vertical quartz reactor with the europium oxide charge (m = 10 g) at room temperature for 30 min. Then, using a programmable regulator, the temperature in the vertical furnace was increased to 1100 °C at the rate of 50 °C/min. After that, the process was carried out at specified parameters for 5 h. A very important condition is to maintain the specified temperature value. A decrease in the synthesis flowrate will result in the appearance of mixed europium sulfide Eu_3S_4 in the samples, while an elevated temperature may lead to the dissociation of europium monosulfide with the formation of non-stoichiometric phases of type EuS_{1-x}. The gases leaving the reactor, in order to absorb toxic components, were alternately passed through saturated aqueous solutions of copper sulfate and sodium hydroxide. After the synthesis stage, the reactor was cooled in the off-furnace mode to room temperature. Then, the heating of carbon disulfide was switched off, but the argon flow was passed through the entire system for an additional 1 h. When the reactor is heated, the occurring process can be described by the equation:

$$2Eu_2O_3 + 3CS_2 \rightarrow 4EuS + 3CO_2 + 2S \quad (1)$$

The polycrystalline product obtained in this way is described by the EuS stoichiometric composition and does not contain any impurities. According to the data of SEM analysis, the powder is formed by uncut particles with sizes in the range of 1–5 μm and, in the particle shapes, a cubic motif can be observed. As it appears, the loss of faceting occurs due to the nature of the anion exchange reaction governed by a continuous diffusion mass transfer in the solid phase.

To evaluate the europium monosulfide oxidation by atmospheric oxygen in the isothermal mode, each charge of 0.5 g EuS was evenly distributed as a thin layer in a flat ceramic boat with the bottom sized 3×5 cm^2. In order not to duplicate the formation of an obstructive layer during the oxidation process, all samples of europium monosulfide were finely ground in an agate mortar for 20 min. Then, all boats, in parallel, were gently inserted into the horizontal furnace and the samples treatment was carried out in the air. When the boat was removed from the furnace, it was cooled to room temperature in a desiccator with a silica gel. The study of the obtained oxidized samples phase composition was performed by the XRD analysis. The experiments were conducted at 400, 500, 600, 700, 800, 900 and 1000 °C. The total oxidation time at each temperature did not exceed 10 h. The samples for XRD analysis were taken from the furnace one by one at the time interval of 1 h. For high temperatures (800–1000 °C), at the initial oxidation stages, the samples were taken after 5, 10, 15 and 30 min. A set of 56 samples was obtained and analyzed.

Methods of physical-chemical analysis

The thermal analysis in the synthetic air (80% Ar-20% O_2) flow was carried out at Simultaneous Thermal Analysis (STA) equipment 499 F5 Jupiter NETZSCH (Germany). The powder samples were inserted into alumina crucibles. The heating rate was 3 °C/min. For the enthalpy determination, the equipment was calibrated with the use of standard metal substances, such as In, Sn, Bi, Zn, Al, Ag, Au, Ni. The heat effect peaks were determined with the package «Proteus 6 2012». The peak temperature and area in parallel experiments were reproduced at the inaccuracy lower than 3%.

The X-ray phase analysis (XRD) was performed on a BRUKER D2 PHASER diffractometer with a linear detector LYNXEYE (CuKα radiation, Ni-filter). The Rietveld refinement of the selected six samples was performed using package TOPAS 4.2 [61]. Almost all peaks were indexed by EuS, Eu_3S_4, Eu_2O_2S, $Eu_2O_2SO_4$ or $Eu_2(SO_4)_3$ phases. The powder diffraction data of $Eu_2O_2SO_4$ for Rietveld analysis were collected at room temperature with a Bruker D8 ADVANCE powder diffractometer (Cu–Kα radiation) and linear VANTEC detector. The step size of 2θ was 0.016° and the counting time was 5 s per step. The electron-microscopy analysis was carried out on an electron microscope JEOL JSM-6510LV. The X-ray energy-dispersive analyzer

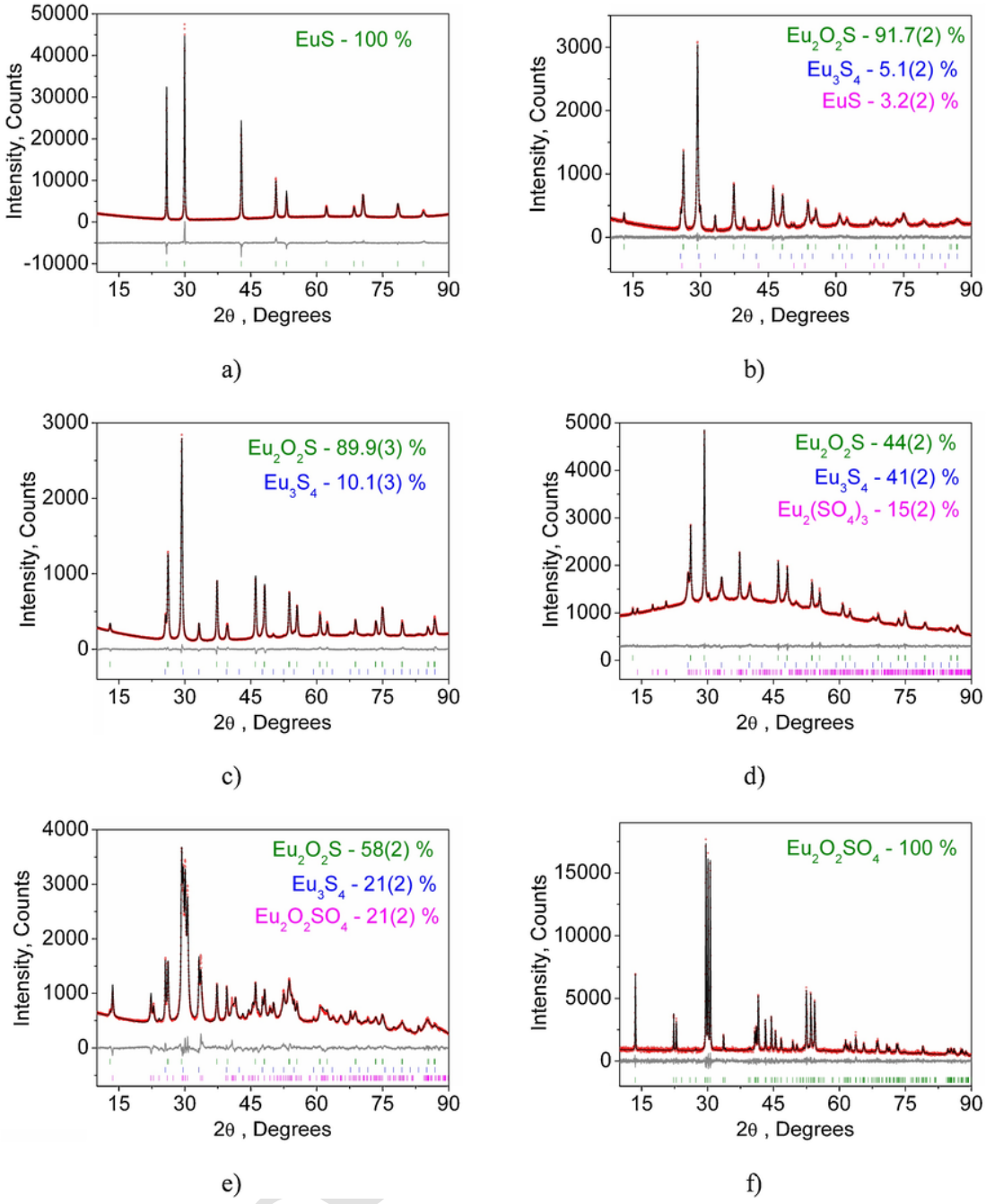

Fig. 2. Difference rietveld plot of: (a) EuS; (b) EuS-Eu_3S_4-Eu_2O_2S; (c) Eu_3S_4-Eu_2O_2S; (d) Eu_3S_4-Eu_2O_2S-$Eu_2(SO_4)_3$; (e) Eu_3S_4-Eu_2O_2S-$Eu_2O_2SO_4$; (f) $Eu_2O_2SO_4$.

was used to register the X-rays at the element spectrum plotting in selected sample surface areas. The element content determination inaccuracy in element content determination was equal to ±0.2%.

The Fourier-transform infrared spectroscopy (FTIR) analysis was carried out at a Fourier Transform Infrared Spectrometer FSM 1201. The sample for the investigation was prepared in the tablet shape with the addition of annealed KBr. The luminescence spectra at room temperature were recorded using a Horiba-Jobin-Yvon T64000 spectrometer. The spectral resolution of the spectrometer measurement channel was 2.7 cm^{-1}. The excitation radiation was the 514.5 nm line of a Spectra Physics Stabilite 2017 laser. The exciting radiation does not fall into exact resonance with any of Eu^{3+} energy levels. However, the off-resonance excitation is found to be quite sufficient in recording the luminescence spectra with a high count rate. High resolution and extreme stability of excitation source were favourable for obtaining high quality luminescence spectra, as was shown in numerous similar studies [10,12,15].

Results and discussion

Dynamic oxidation of EuS

The differential-thermal analysis of europium monosulfide in the atmosphere of synthetic air shows that the EuS oxidation occurs over

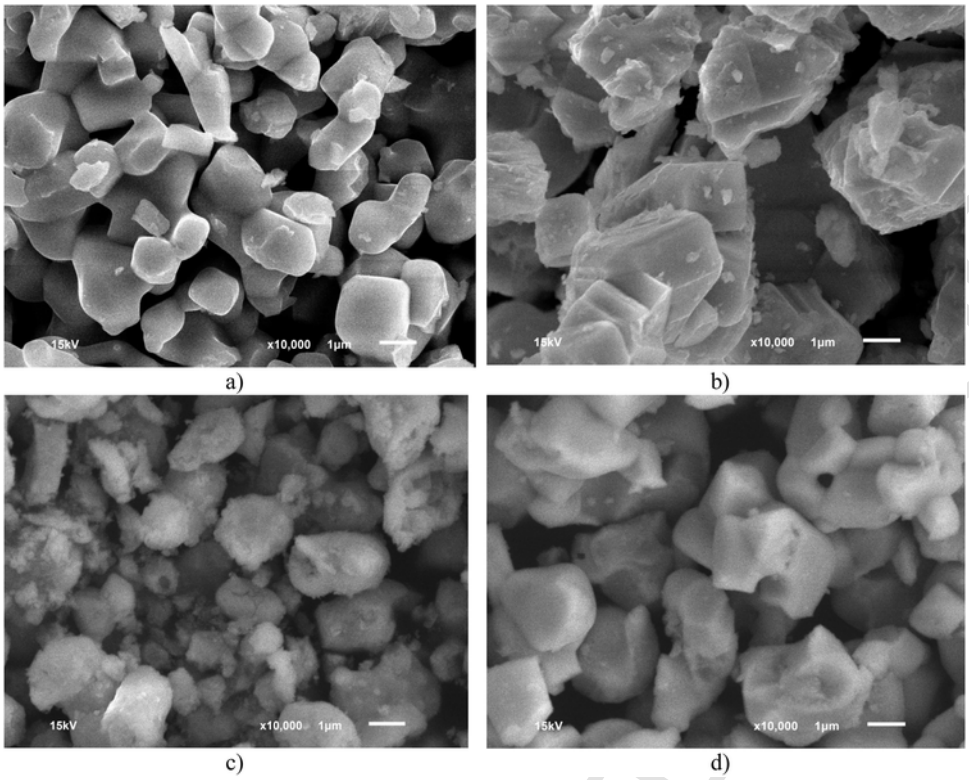

Fig. 3. The transformation of particles during the oxidation of europium monosulfide, depending on the process temperature: (a) 25 °C (EuS); (b) 500 °C (EuS-Eu_3S_4-Eu_2O_2S); (c) 700 °C (EuS-Eu_3S_4-Eu_2O_2S-$Eu_2O_2SO_4$); (d) 800 °C ($Eu_2O_2SO_4$).

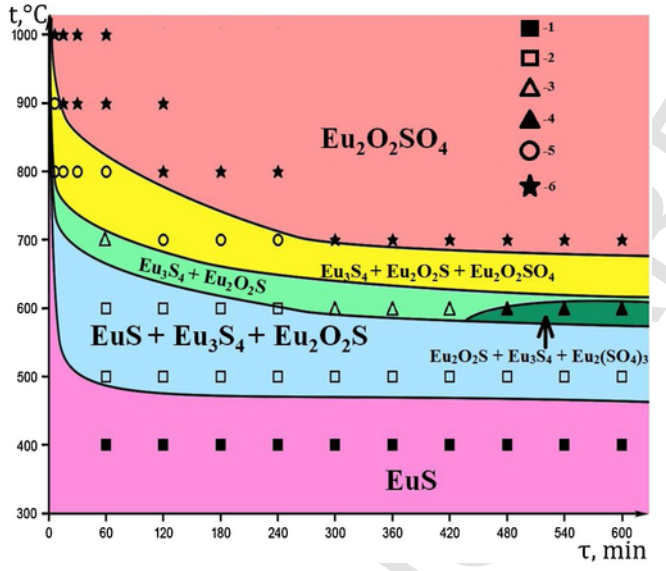

Fig. 4. Kinetic scheme of changes in the chemical composition of the samples during oxidation of europium monosulfide with air oxygen. Legend: 1-EuS; 2-EuS + Eu_3S_4 + Eu_2O_2S; 3-Eu_3S_4 + Eu_2O_2S; 4-Eu_3S_4 + Eu_2O_2S + $Eu_2(SO_4)_3$; 5-Eu_3S_4 + Eu_2O_2S + $Eu_2O_2SO_4$; 6-$Eu_2O_2SO_4$.

a wide temperature range, as shown in Fig. 1. Up to 500 °C, there are no changes in the TG and DTA curves. Starting from 500 °C, the increase in the mass of the sample and a slight heat release are recorded. A plateau appears on the DTA curve in the temperature range of 700–800 °C, which indicates a uniform flow of the process in this temperature range. Starting at 830 °C, a powerful heat release is fixed on the DTA curve. The maximum of the thermal effect is at 875 °C. The oxidation process is completed at 970 °C: the TG curve goes to the plateau, the DTA curve comes to a steady state. The mass gain at the process termination corresponds to the europium oxysulfate $Eu_2O_2SO_4$ formation by the reaction:

$$2EuS + 4O_2 \rightarrow Eu_2O_2SO_4 + SO_2 \quad (2)$$

However, the nature of the DTA curve does not allow describing the reaction as a one-stage process. Obviously, the processes occurring in the temperature ranges of 500–800 °C and 800–1000 °C correspond to different chemical reactions. Having the data on the enthalpies of the formation of all compounds which formation can be assumed in the oxidation process [45,62,63], the enthalpy of the process was calculated by the equation:

$$2EuS_{(cub)} + 4O_{2(gas)} \rightarrow Eu_2O_2SO_{4(monocl)} + SO_{2(gas)} \quad (3)$$

The calculated enthalpy of reaction $\Delta H^0_{calc} = ——1731.1$ kJ/mol is in good relation to the experimentally determined value $\Delta H^0_{exp} = ——1718.5$ kJ/mol.

Isothermal oxidation

At 400 °C, there are no changes in the qualitative phase composition of the samples for 10 h and all samples contain pure EuS (Fig. 2a). At 500 °C, the samples principally change their phase composition. After 1 h of the interaction with the air at this temperature, the sample contains a mixture of EuS, Eu_3S_4 and Eu_2O_2S. During 10 h of oxidation process for, the qualitative phase composition of the sam-

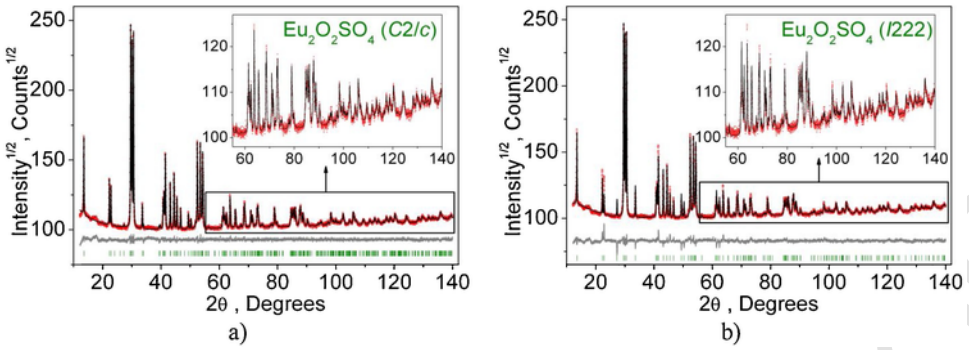

Fig. 5. Difference rietveld plot of $Eu_2O_2SO_4$ by two different structural models: (a) *C*2/*c*; (b) *I*222.

Table 1
Main parameters of processing and refinement of the $Eu_2O_2SO_4$ sample.

Compound	$Eu_2O_2SO_4$	
Sp.Gr.	*C*2/*c*	*I*222
a, Å	13.6583 (3)	4.0716 (1)
b, Å	4.18874 (7)	4.1883 (1)
c, Å	8.1440 (1)	13.0412 (3)
β, °	107.292 (2)	–
V, Å^3	444.89 (2)	222.393 (9)
Z	4	2
2*θ*-interval, °	12–140	12–140
No. of refined structural parameters	16	8
R_{wp}, %	1.37	1.77
R_p, %	1.04	1.25
R_{exp}, %	0.93	0.93
χ^2	1.47	1.90
R_B, %	0.26	1.21

ples does not change, but the relative intensity of the reflexes of each phase changes and it indicates a variation in the phase percentage in the samples formed at 500 °C (Fig. 2b). With a process time increase, the content of EuS gradually decreases and the content of mixed sulfide Eu_3S_4 and oxysulfide Eu_2O_2S increases. It was not possible to reach the complete oxidation of EuS to oxide reaction products even for 10 h.

However, carrying out the process at 600 °C, it is possible to completely oxidize the EuS sample to reaction products Eu_3S_4 and Eu_2O_2S for 5 h (Fig. 2c). Treating the EuS samples at this temperature up to 7 h does not lead to a change in the phase composition. However, after the treatment for 8 h, the impurities of europium (III) sulfate $Eu_2(SO_4)_3$ are detected (Fig. 2d). The increase of the interaction time to 10 h results in an increase of the content of europium sulfate and oxysulfide in the samples and in a decrease of the content of mixed sulfide Eu_3S_4, which makes it possible to describe this process by the equation:

$$2Eu_3S_4 + 8O_2 \rightarrow 2Eu_2(SO_4)_3 + Eu_2O_2S + SO_2 \quad (4)$$

This change is characterized by the occurrence of a kinetically hindered oxidation of Eu_3S_4. Carrying out the process at 700 °C allows oxidizing the sample to a mixture of mixed sulfide and europium oxysulfide Eu_2O_2S for 1 h of the interaction with the air. Starting from the second hour of oxidation, europium oxysulfate $Eu_2O_2SO_4$ begins to appear in the samples (Fig. 2e). The oxysulfate formation rate is so great that, by the fifth hour and further, the samples are $Eu_2O_2SO_4$ single-phase powders.

At 800 °C, after the five-minute processing, three phases are observed in the sample: Eu_3S_4, Eu_2O_2S, $Eu_2O_2SO_4$. An increase in the process time to 1 h leads to an increase in the europium oxysulfate content with a simultaneous decrease in the content of sulfides. The sample obtained after 2 h of the oxidation at 800 °C and subsequent samples are single-phase europium oxysulfate $Eu_2O_2SO_4$ powders. After 5 min of the operation at 900 °C, the sample contains a mixture of three phases: Eu_3S_4, Eu_2O_2S, $Eu_2O_2SO_4$ with an obvious predominance of the oxysulfate component. In 15 min, all further samples are single-phase powders of europium oxysulfate. The samples obtained by the EuS oxidation at 1000 °C for 5 min-10 h are europium oxysulfate $Eu_2O_2SO_4$ single-phase powders (Fig. 2f).

According to the data of electron microscopy, a tendency to the particles loosening is observed during the decomposition process. Europium (II) sulfide is formed by grains sized ˜1 μm (Fig. 3a). The particle cracks are weakly seen. The cubic motif can be found only in the

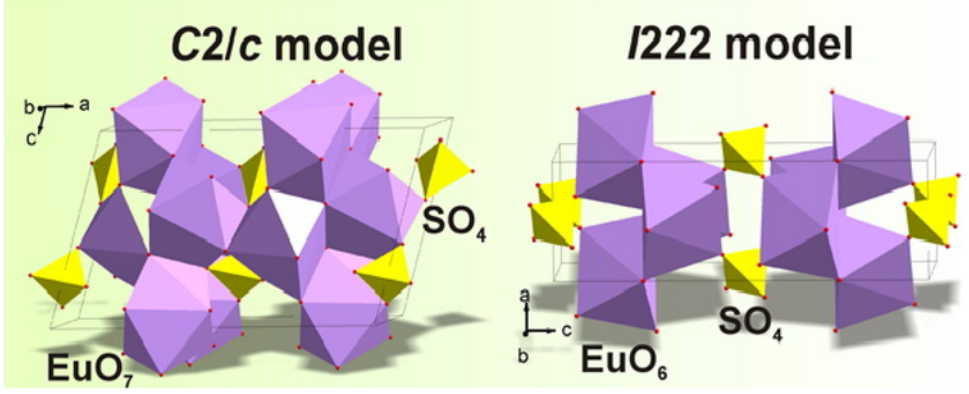

Fig. 6. Crystal structures of $Eu_2O_2SO_4$ in two different structural models *C*2/*c* and *I*222.Fig.7. Infrared spectra of $Eu_2O_2SO_4$.

Table 2
Correlation diagrams for internal vibrations of SO_4 tetrahedra in the *C*2/*c* and *I*222 structural models for $Eu_2O_2SO_4$.

*C*2/*c* model			
Wavenumber, cm^{-1} [1]	T_d point group	C_2 site symmetry	C_{2h} factor group symmetry
983	A_1 (ν_1)	A	A_g+A_u
450	$E(\nu_2)$	$2A$	$2A_g+2A_u$
1105	$E(\nu_3)$	$A+2B$	$A_g+A_u+2B_g+2B_u$
611	$E(\nu_4)$	$A+2B$	$A_g+A_u+2B_g+2B_u$
*I*222 model			
Wavenumber, cm^{-1} [1]	T_d point group	D_2 site symmetry	D_2 factor group symmetry
983	A_1 (ν_1)	A	A
450	$E(\nu_2)$	$2A$	$2A$
1105	$E(\nu_3)$	$B_1+B_2+B_3$	$B_1+B_2+B_3$
611	$E(\nu_4)$	$B_1+B_2+B_3$	$B_1+B_2+B_3$

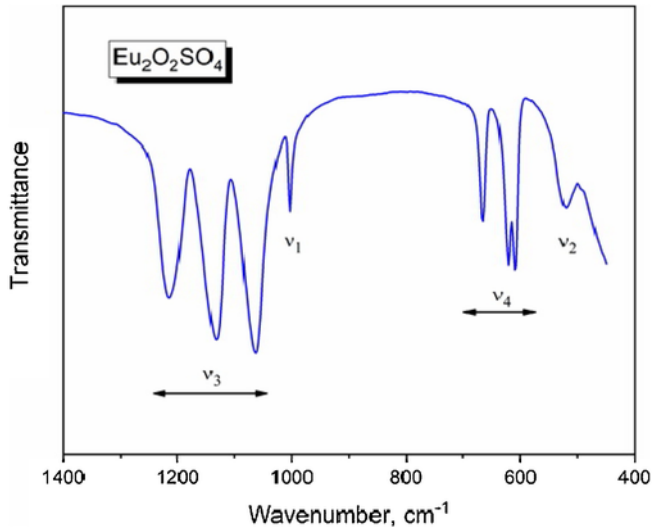

Fig. 7. Infrared spectra of $Eu_2O_2SO_4$.

shapes of some particles. In the oxidation process, the growth of nanocrystals of reaction products begins at the particle surfaces. Respectively, particle destruction is evident. The temperature increase induces a complete damage of the particles and the formation of the samples that consist predominantly of the X-ray amorphous phase. However, at high temperatures (>900 °C), the tendency to the aggregation of particles and the formation of microparticles with a monoclinic motif becomes vivid (Fig. 3d).

According to the SEM analysis, a tendency to the particle destruction is observed during the chemical decomposition process. Europium (II) sulfide is formed by the grains sized about 1 μm (Fig. 3a). The particles cut is weakly expressed. The cubic motif is seen only in the structure of some of them. In the oxidation process, the growth of nanocrystals of reaction products begins at the particle surface. The particles loosen and exfoliate (Fig. 3b). An increase in temperature leads to complete disintegration of the particles and the formation of the samples that consist predominantly of the X-ray amorphous phase (Fig. 3c). However, at high temperatures (>900 °C), the tendency to particles aggregation and the formation of microparticles with a monoclinic motif become vivid (Fig. 3d). In the process of EuS oxidation under isothermal conditions, the samples of six different phase compositions were obtained. The phase composition dependence on the temperature/time conditions is presented in Fig. 4. The processes occurring in the temperature range of 500–600 °C are kinetically hindered. At 500 °C, it was impossible to oxidize EuS for 10 h completely and residual EuS was always detected in the samples.

At 600 °C, the EuS sample was completely oxidized for 5 h (to a mixture of $Eu_3S_4 + Eu_2O_2S$). In three hours, after reaching the equilibrium state, at the same temperature, another clearly kinetically hindered process is initiated: the oxidation of mixed europium sulfide Eu_3S_4 with the formation of europium (III) sulfate $Eu_2(SO_4)_3$. In the system, at a given temperature (600 °C), europium completely transforms into the trivalent state. Starting from 700 °C, this kinetically hindered process is replaced by the process of combined oxidation of mixed sulfide and oxysulfide to oxysulfate. This process is completed for 5 h. With a further increase in temperature, the oxidation proceeds only according to this scheme, but the stages change each other much quicker. Thus, the EuS oxidation is a two-stage process: $EuS \rightarrow Eu_3S_4 + Eu_2O_2S \rightarrow Eu_2O_2SO_4$. According to DTA, in the second stage, the oxidation of two intermediate compounds proceeds in parallel. However, it can be assumed that Eu_3S_4 containing europium in its divalent state is the first to enter this process.

Structural and spectroscopic properties of $Eu_2O_2SO_4$

One of the main oxidation products of europium monosulfide is oxysulfate $Eu_2O_2SO_4$. However, the correct diffraction identification of this product is rather tricky. The structure refinement for $Eu_2O_2SO_4$ was performed by Rietveld method. The recorded XRD pattern is shown in Fig. 5. Almost all peaks can be indexed by a monoclinic cell (*C*2/*c*) with parameters close to $Eu_2O_2SO_4$ [64] or by a higher symmetry orthorhombic cell (*I*222) with parameters close to $Nd_2O_2SO_4$ [65]. Therefore, these two structure models were tested for the Rietveld refinements. The Nd ion site was replaced by Eu. The refinements were stable and gave low *R*-factors (Table 1, Fig. 5). The coordinates of atoms and main bond lengths are given in Tables S5 and S6, respectively. Both refined models were tested with the checkCIF internet tool (https://checkcif.iucr.org/) and no serious problems (Alert A or Alert B types) were found in the structures. Also, the difference plots are adequate for both cases, despite a much better quality of the difference plot observed in the *C*2/*c* model. The *I*222 model is of a higher symmetry than that of the *C*2/*c* model; also, the *I*222 model has a twice smaller cell volume and twice smaller number of refined parameters than those of the *C*2/*c* model (Fig. 6). However, the best fit with an evidently smaller R-factor was obtained within the *C*2/*c* model. In this situation, choosing the correct model becomes a challenge. This was a reason why it was decided to make IR calculations for the structures obtained in both models.

The free tetrahedral SO_4^{2-} ion with the T_d symmetry exhibits four internal vibrations. All four vibrations are Raman-active, whereas only ν_3 and ν_4 are infrared-active. In the solid state, ν_3 and ν_4 may split into two or three bands because of the site effect [66]. In Table 2, the correlation is given between the free SO_4^{2-} ion vibrations in the

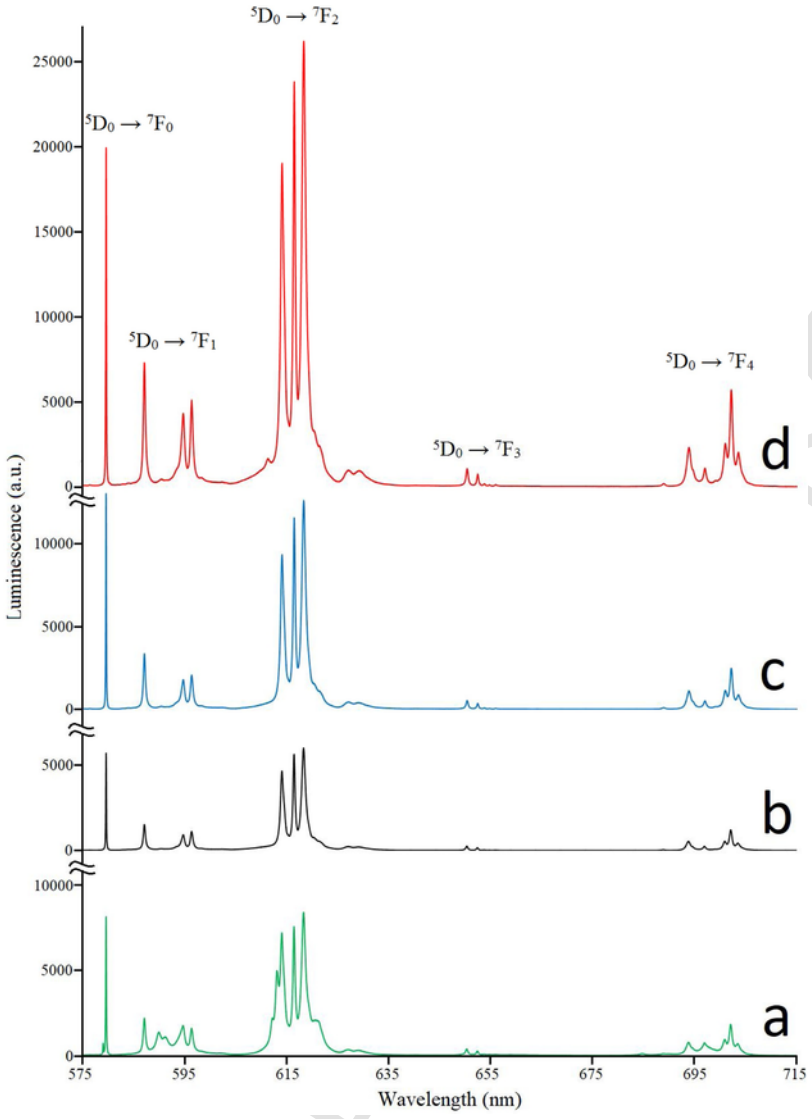

Fig. 8. The luminescence spectra of $Eu_2O_2SO_4$ samples obtained at different oxidation temperatures of europium sulfide are: (a) 700 °C, (b) 800 °C, (c) 900 °C, (d) 1000 °C.

Td symmetry and the SO_4 internal vibrations in the case of monoclinic (*C*2/*c*) and orthorhombic (*I*222) cells in $Eu_2O_2SO_4$. The vibrational irreducible representations for the monoclinic structure at the center of the Brillouin zone is $\Gamma_{vibr} = 13A_g + 13A_u + 14B_g + 14B_u$, where $A_u + 2B_u$ are acoustic modes, $13A_g + 14B_g$ are Raman-active, while $12A_u + 12B_u$ modes are active in IR spectra. In the case of orthorhombic structure, the vibrational irreducible representations at the center of Brillouin zone is $\Gamma_{vibr} = 5A + 6B_1 + 8B_2 + 8B_3$, where $B_1 + B_2 + B_3$ are acoustic modes, $5A + 5B_1 + 7B_2 + 7B_3$ are Raman-active modes, while $5B_1 + 7B_2 + 7B_3$ modes are active in IR spectra. From the correlation diagrams and vibrational irreducible representations, we can conclude that four spectral bands should be observed in the range of stretching vibrations of SO_4 tetrahedra in Raman spectra as in the case of monoclinic and in the case of orthorhombic structures. The infrared spectra of the *C*2/*c* structure should contain four bands in this region, while the symmetric stretching *A* mode is forbidden in the case of orthorhombic structure and only three spectral bands should be observed. Thus, the recorded IR spectrum of $Eu_2O_2SO_4$, as shown in Fig. 7, corresponds to the monoclinic *C*2/*c* structure.

The luminescence spectra of the $Eu_2O_2SO_4$ samples fabricated at different annealing temperatures (700, 800, 900 and 1000 °C) were recorded using excitation wavelength 514.5 nm at spectral resolution 2.7 cm^{-1}. The samples were taken in approximately equal quantities in order to enable a qualitative comparison of the luminescent intensities between them. All spectra are similar at first sight, containing their characteristic luminescent bands of the Eu^{3+} ion at transitions $^5D_0 \rightarrow {}^7FJ$ (J = 0–4) [10,12,67,68]. The transitions with J = 5,6 were also observed, but their intensity was too small to be shown in Fig. 8. Among four recorded spectra, the three ones taken from the samples oxidized at higher temperatures (from 800 to 1000 °C), exhibit their almost identical shapes of intraband crystal field splitting, while the luminescence intensity grows with the oxidation temperature increase. The most pronounced intensity growth can be observed for the sample oxidized at 900 °C in comparison to that oxidized at 800 °C (2.8 times maximum peak intensities). This intensity behavior is typical of the annealing of different crystalline phosphors and is commonly

treated as the effect of a better crystallinity reached at higher temperatures.

The luminescence spectrum of the sample oxidized at 700 °C shows certain differences in its band shapes, concerning the samples obtained at higher temperatures. First of all, the region of ultranarrow transition $^5D_0 \rightarrow {}^7F_0$ contains two peaks, as can be seen in Fig. S4. In Fig. S4, are the ultranarrow lines in the samples annealed at 700 and 800 °C, as well as the same line in recently studied $Eu_2(SO_4)_3$ [12]. The latter spectrum is featured by the ultranarrow line position coinciding with one of the peaks in the spectrum of the sample annealed at 700 °C, while the sample annealed at 800 °C contains a single ultranarrow line coinciding with the more intense component in the spectrum of the sample annealed at 700 °C. Therefore, the ultranarrow line at 579.6 nm must be ascribed to $Eu_2O_2SO_4$ in both samples under study, while the ultranarrow component at 579.0 nm in the sample annealed at 700 °C must be ascribed to the impurity of $Eu_2(SO_4)_3$. Curious is that the ultranarrow line in the impurity $Eu_2(SO_4)_3$ is almost completely symmetric and it evidence its good crystalline quality, in comparison with the asymmetric line in pure $Eu_2(SO_4)_3$ [12]. The presence of the $Eu_2(SO_4)_3$ impurity in the sample annealed at 700 °C also influences the rest of its luminescent bands, as illustrated in Fig. S5, where the comparison of this sample spectrum with that of the sample annealed at 800 °C is presented. However, the subtraction of the 800 °C sample spectrum multiplied by the adjustable factor being 0.78 in our case, from the 700 °C sample spectrum results in the spectrum well coinciding with that of $Eu_2(SO_4)_3$ (Fig. S6). Therefore, the sample annealed at 700 °C is likely to contain 78% of $Eu_2O_2SO_4$ and 22% of $Eu_2(SO_4)_3$.

The europium sulfate formation occurs following Eq. 4. The absence of spectral lines of europium oxysulfide is due to its instability at given temperatures and, vice versa, according to the equation:

$$Eu_2O_2S + 2O_2 \rightarrow Eu_2O_2SO_4 \quad (5)$$

It was not possible to detect the $Eu_2(SO_4)_3$ impurity by X-ray diffraction analysis due to the low crystallinity of the samples.

Conclusions

Thus, in the present study, the process of EuS high-temperature oxidation with atmospheric oxygen, in dynamic and isothermal modes, has been observed. It is established that the oxidation proceeds in two stages and is associated with several topochemical processes of varying complexity degrees. The applicability of EuS oxidation as a method for the synthesis of europium oxysulfate $Eu_2O_2SO_4$ is established. According to the luminescence spectroscopy data, the synthesis temperature has a significant effect on the luminescence intensity in the $Eu_2O_2SO_4$ samples, in view of different crystallinity degrees. It was clearly established that the structural analysis of $Eu_2O_2SO_4$ is possible only by combining the diffraction and spectroscopic methods. The future activities can be aimed at the synthesis of catalytically active $Eu_2O_2SO_4$ powders in a nanostructure by the oxidation of EuS nanopowders.

Acknowledgements

The authors are grateful for the support from RFBR (16-52-48010, 18-02-00754, 18-08-00985 and 18-32-20011). The work was supported by Act 211 Government of the Russian Federation, contract № 02.A03.21.0011. Additionally the work was partially supported by the Ministry of Science and Higher Education of the Russian Federation (4.1346.2017/4.6).

Appendix A. Supplementary data

Supplementary material related to this article can be found, in the online version, at doi:https://doi.org/10.1016/j.jiec.2019.05.006.

References

[1] Shuxing Li, Daiming Tang Le Wang, Yujin Cho, Xuejian Liu, Xingtai Zhou, Lu Lu, Lin Zhang, Takashi Takeda, Naoto Hirosaki, Rong-Jun Xie, Chem. Mater. 30 (2) (2017) 494.
[2] Xiaofei Shi, Zhihao Wang, Toshiaki Takei, Xuejiao Wang, Qi Zhu, Xiaodong Li, Byung-Nam Kim, Xudong Sun, Ji-Guang Li, Inorg. Chem. 57 (11) (2018) 6632.
[3] Chunling Li, Xueling Fan, Peng Jiang, Xiaochao Jin, Mater. Lett. 222 (2018) 41.
[4] F. Baur, T. Jüstel, J. Lum. 196 (2018) 431.
[5] M. Behrendt, S. Mahlik, M. Grinberg, D. Stefanska, P.J. Deren, Opt. Mater. 63 (2017) 158.
M. Puchalska, Opt. Mater. 72, 2017, 452.
[7] M.A. van de Haar, J. Werner, N. Kratz, T. Hilgerink, M. Tachikirt, J. Honold, M.R. Kramers, App. Phys. Lett. 112 (13) (2018) 132101.
[8] R. Laishram, U. Maitra, Chem. Select. 3 (2) (2018) 519.
[9] Pinglu Shi, Zhiguo Xia, Maxim S. Molokeev, Victor V. Atuchin, Dalton Trans. 43 (25) (2014) 9669.
[10] V.V. Atuchin, A.S. Aleksandrovsky, O.D. Chimitova, T.A. Gavrilova, A.S. Krylov, M.S. Molokeev, A.S. Oreshonkov, B.G. Bazarov, J.G. Bazarova, J. Phys. Chem. C 118 (28) (2014) 15404.
[11] Haipeng Ji, Zhaohui Huang, Zhiguo Xia, Maxim S. Molokeev, Xingxing Jang, Zheshuai Lin, Victor V. Atuchin, Dalton Trans. 44 (16) (2015) 7679.
[12] Yu.G. Denisenko, A.S. Aleksandrovsky, V.V. Atuchin, A.S. Krylov, M.S. Molokeev, A.S. Oreshonkov, N.P. Shestakov, O.V. Andreev, J. Indust. Eng. Chem. 68 (2018) 109.
[13] A.H. Reshak, Z.A. Alahmed, J. Bila, V.V. Atuchin, B.G. Bazarov, O.D. Chimitova, M.S. Molokeev, I.P. Prosvirin, A.P. Yelisseyev, J. Phys. Chem. C. 120 (19) (2016) 10559.
[14] Xuejiao Wang, Maxim S. Molokeev, Qi Zhu, Ji-Guang Li, Chem. Europ. J. 23 (2017) 16034.
[15] V.V. Atuchin, A.K. Subanakov, A.S. Aleksandrovsky, B.G. Bazarov, J.G. Bazarova, T.A. Gavrilova, A.S. Krulov, M.S. Molokeev, A.S. Oreshonkov, S. Yu, Mater. Des. 140 (2018) 488.
[16] Myung Ho Choi, Min Kyung Kim, Vin Na Jo, Dong Woo Lee, I.I. Wun Shim, Kang Min Ok, Bull. Korean Chem. Soc. 31 (4) (2010) 1077.
[17] L. Paama, I. Pitkanen, J. Valkonen, E. Parnoja, H. Kola, P. Peramaki, Talanta 67 (5) (2005) 897.
[18] Xu Yan, Shaohua Ding, Xuefang Zheng, J. Sol. State Chem 180 (7) (2007) 2020.
[19] Yu.G. Denisenko, V.V. Atuchin, M.S. Molokeev, A.S. Aleksandrovsky, A.S. Krylov, A.S. Oreshonkov, S.S. Volkova, O.V. Andreev, Inorg. Chem. 57 (21) (2018) 13279.
[20] X. Zhang, Yu. Ma, H. Zhao, C. Jiang, Yu. Sun, Ya. Xu, J. Struct. Chem. 52 (5) (2011) 954.
[21] Fashen Chen, Gen Chen, Tao Liu, Ning Zhang, Xiaohe Liu, Hongmei Luo, Junhui Li, Limiao Chen, Renzhi Ma, Guanzhou Qiu, Sci. Reports 5 (2015) 17934.
[22] M. Shaterian, M.A. Rezvani, V. Shahsavandi, K. Qasemi, J. Nanostruct. 7 (2) (2017) 97.
[23] Danyang Ma, Chungen Li, Lei Wang, Hao Liu, Shengliang Zhong, Yuan Li, J. Nanoparticle Res. 19 (10) (2017) 341.
[24] W. Paul, J. Magn. Magn. Mater. 87 (1990) 23.
[25] Jinbao Lian, Xudong Sun, Xiaodong Li, Mater. Chem. Phys. 125 (2011) 479.
[26] I. Valsamakis, M. Flytzani-Stephanopoulos, Appl. Cat. B: Environ. 106 (2011) 255.
[27] S. Tan, S.N. Paglieri, D. Li, Cat. Comm. 73 (2016) 16.
[28] F.J.A. Loureiro, T. Yang, D.G. Stroppa, D.P. Fagg, J. Mater. Chem. A. 3 (24) (2015) 12636.
[29] P.V.M. Dixini, V.G. Celante, M.F.F. Lelis, M.B.J.G. Freitas, J. Power Sources. 260 (2014) 163.
[30] W. Zhang, I.W.C.E. Arends, K. Djanashvili, Dalton Trans. 45 (36) (2016) 14019.
[31] Keita Ikeue, Tomoatsu Kawano, Masakazu Eto, Dongjie Zhang, Masato Machida, J. Alloys Compd. 451 (1–2) (2008) 338.
[32] Dongjie Zhang, Takahiro Kawada, Fumihiko Yoshioka, Masato Machida, ACS Omega 1 (5) (2016) 789.
[33] S. Kim, T. Masui, N. Imanaka, Electrochemistry 77 (8) (2009) 611.

[34] Fan Liu, Jing Bao Lian, Xu Guang Xi, Wu Nian Chu, Solid State Phenom. 281 (2018) 679.
[35] Jingbao Lian, Fan Liu, Jing Zhang, Yanyu Yang, Xuri Wang, Zhaoren Zhang, Feng Liu, Optik 127 (20) (2016) 8621.
[36] Xing Li, Jingbao Lian, Optik 127 (1) (2016) 401.
[37] Jinbao Lian, Hua Qin, Ping Liang, Feng Liu, Sol. State Sci. 48 (2015) 147.
[38] Jingbao Lian, Feng Liu, Xuejiao Wang, Xudong Sun, Powder Techn. 253 (2014) 187.
[39] Jingbao Lian, Ping Liang, Bingxin Wang, Feng Liu, J. Ceram. Process. Res. 15 (2014) 382.
[40] Guangxi Xu, Fan Liu, Jingbao Lian, Nianchu Wu, Xue Zhang, Jiao He, Ceram. Int. 44 (15) (2018) 19070.
[41] O.V. Andreev, Yu.G. Denisenko, E.I. Sal'nikova, N.A. Khritokhin, K.S. Zyryanova, Russ. J. Inorg. Chem. 61 (3) (2016) 296.
[42] O.V. Andreev, I.A. Razumkova, A.N. Boiko, J. Fluor. Chem. 207 (2018) 77.
[43] I.A. Razumkova, J. Fluor. Chem. 205 (2018) 1.
Yu.G. Denisenko, N.A. Khritokhin, O.V. Andreev, S.A. Basova, E.I. Sal'nikova, A.A. Polkovnikov, J. Sol. State Chem. 255, 2017, 219.
H. Stark, R.L.N. Yatavelli, S.L. Thompson, H. Kang, J.E. Krechmer, J.R. Kimmel, B.B. Palm, W. Hu, P.L. Hayes, D.A. Day, P. Campuzano-Jost, M.R. Canagaranta, J.T. Jayne, D.R. Worsnop, J.L. Jimenes, Environ. Sci. Technol. 51 (15), 2017, 8491.
[46] P. Povea, J.L. Arroyo, G. Carreno, A. Norambuena, P.L. Rios, M.B. Camarada, I. Chavez, J.M. Manriquez, C. Morales-Verdejo, Thermochim. Acta 666 (2018) 181.
[47] X. Liu, K.A. Salmeia, D. Rentsch, J. Hao, S. Gaan, Appl. Pyrolysis 124 (2017) 219.
[48] M. Unni, A.M. Uhl, S. Savliwala, B.H. Savitzky, R. Dhavalikar, N. Garraud, D.P. Arnold, L.F. Kourkoutis, J.S. Andrew, C. Rinaldi, ACS Nano. 11 (2) (2017) 2284.
[49] J.L. Jambor, D.K. Nordstrom, C.N. Alpers, Rev. Mineral. Geochem. 40 (1) (2000) 303.
[50] Y.L. Suponitskii, G.M. Kuz'micheva, A.A. Eliseev, Russ. Chem. Rev. 57 (3) (1988) 209.
K. Ikeue, T. Kawano, D. Zhang, M. Eto, M. Machida, Chemistry 25 (B), 2007, 30.
[52] W.H. Shen, S. Naito, Adv. Mater. Res. 886 (2014) 196.
[53] M. Miura, H. Hirata, K. Ishibashi, M. Machida, SAE Technical Paper. (2009), 2009-01-1071.
[54] M. Machida, T. Kawano, M. Eto, D. Zhang, K. Ikeue, Chem. Mater. 19 (4) (2007) 954.
[55] M. Machida, K. Kawamura, K. Ito, K. Ikeue, Chem. Mater. 17 (6) (2005) 1487.
[56] R.A. Lidin, V.A. Molochko, L.L. Andreeva, Inorganic Chemistry in Reactions: a Handbook, Drofa, Moscow., 2007.
[57] N.N. Greenwood, A. Earnshaw, Chemistry of the Elements, Elsevier, 2012.
[58] Yu.D. Tret'yakov, L.I. Martynenko, A.N. Grigor'ev, A. Yu, Tsivadze, Inorganic Chemistry. Chemistry of the Elements, Textbook for Universities, Chemistry, Moscow, 2001.
[59] Z.K. Heiba, Y. Akin, W. Sigmund, Y.S. Hascicek, J. Appl. Cryst. 36 (6) (2003) 1411.
[60] R.W.G. Wyckoff, In: second edition, Crystal Structures, 1, 1963, p. 85.
[61] Bruker AXS TOPAS V4: General profile and structure analysis software for powder diffraction data. – User's Manual, Bruker AXS, Karlsruhe, Germany, 2008.
[62] O.D. McMasters, K.A. Gschneidner, E. Kaldis, G. Sampietro, J. Chem. Thermod. 6 (9) (1974) 845.
[63] J.R. Eckman, F.D. Rossini, Bureau Standards J. Res. 3 (1929) 597.
[64] I. Hartenbach, T. Schleid, Z. Anorg. Allgem. Chem. 628 (9-10) (2002) 2171.
[65] N.N. Golovnev, M.S. Molokeev, S.N. Vereshchagin, V.V. Atuchin, J. Coord. Chem 68 (11) (2015) 1865.
[66] K. Nakamoto, Infrared and Raman Spectra of Inorganic and Coordination Compounds, 6th edn., Wiley, New York etc., 2009.
[67] Xuejiao Wang, Xiaofei Shi, Maxim S. Molokeev, Zhihao Wang, Qi Zhu, Xiaodong Li, Xudong Sun, Ji-Guang Li, Inorg. Chem. 57 (21) (2018) 13606.
[68] V.V. Atuchin, A.S. Aleksandrovsky, B.G. Bazarov, J.G. Bazarova, O.D. Chimitova, Yu.G. Denisenko, T.A. Gavrilova, A.S. Krylov, E.A. Maximovskiy, M.S. Molokeev, A.S. Oreshonkov, A.M. Pugachev, N.V. Surovtsev, J. Alloys Compd. 785 (2019) 692.